View Article Online
DOI: 10.1039/C7DT00069C

Dalton Transactions

ARTICLE

Slow Magnetic Relaxations in a Ladder-Type Dy(III) Complex and its Dinuclear Analogue

Received 00th January 20xx,

Accepted 00th January 20xx

DOI: 10.1039/x0xx00000x

www.rsc.org/

R. Boča,[a] M. Stolárová Pataky,[b] L. R. Falvello,[c] M. Tomás,[d] J. Titiš[a] and J. Černák[b,*]

The complex $\{[Dy_2(PDOA)_3(H_2O)_6]\cdot 2H_2O\}_n$ (**1**) (H_2PDOA = 1,2-phenylenedioxydiacetic acid) was prepared from aqueous solution. Its crystal structure, built up of {-Dy-O-C-O-}$_n$ chains interlinked by PDOA ligands yielding a ladder-like arrangement, was determined at 173 K. **1** exhibits slow magnetic relaxation under a small magnetic field B_{DC} = 0.2 T with two (LF and HF) relaxation channels. The LF relaxation time at B_{DC} = 0.2 T and T = 1.85 K is as slow as τ(LF) = 46 ms whereas the HF channel is τ(HF) = 1.4 ms. The mole fraction of the LF species is x_{LF} = 0.76 at 1.85 K and it escapes progressively on heating. In the dinuclear analogue $[Dy_2(PDOA)_3(H_2O)_6]\cdot 3.5H_2O$ (**2**) one PDOA ligand forms a bis(chelate) bridge between the two Dy(III) atoms yielding a local structure analogous to that in **1**; however its AC susceptibility data shows slightly different quantitative characteristics of the single-molecule magnetic behaviour.

Introduction

The class of single molecule magnets (including single chain and single ion magnets) has attracted much attention in the last decade because of promising technical applications.[1] Research moved from the assembly of 3d-metal complexes in earlier stages (like the well known Mn_{12} or Fe_8 plate-like complexes) to 4f systems, and to mixed 3d-4f systems more recently.[2] Among these investigations a prominent role has been played by Dy(III) complexes because of the large magnetic moment and strong magnetic anisotropy that play a key role in creating an efficient barrier to spin reversal.[3] The Dy(III) complexes studied to date comprise mononuclear complexes,[4] dinuclear species[5] or complexes exhibiting higher nuclearity including polymeric complexes.[6] Much attention was also given to 3d-Dy(III) heterometallic complexes with various dimensionalities.[7] The studied Dy(III) complexes with SMM behaviour display variable values of the spin reversal barrier, and among them the reported record spin reversal barrier was over 1000 K.[8] On the other hand, currently the blocking temperatures, with maximum values of about 20 K, are still rather low.[3]

The synthesis, room temperature crystal structure, thermal and photoluminescence properties of $\{[Dy_2(PDOA)_3(H_2O)_6]\cdot 2H_2O\}_n$ (H_2PDOA = 1,2-phenylenedioxy-diacetic acid), hereafter **1**, have been reported previously.[9] H_2PDOA after deprotonation to the dianion is an efficient multidentate O-donor ligand which can act as a tetradentate chelating ligand,[10] as a penta-,[11] hexa-[12] and even heptadentate[13] chelating-bridging ligand, or simply as a long bridge in a bis(chelate)[10a,11c] or bis(monodentate) fashion[11a,11c]; in most reported crystal structures bearing the PDOA ligand and a lanthanoid central atom, two PDOA ligands with different structural (chelating and bridging) functions are present resulting in dinuclear or polymeric structures.[10a,11]

As a continuation of our broader quest for complexes displaying SMM behaviour,[14] here we report the crystal structure redetermination at 173 K along with the DC and AC magnetic data of **1**. The structural and magnetic data are compared with a novel dinuclear complex $[Dy_2(PDOA)_3(H_2O)_6]\cdot 3.5H_2O$, **2**, which is an analogue of **1**.

Experimental

Materials and methods

All commercial chemicals were used as received without further purification. The infrared (IR) spectra were collected on a Perkin Elmer Spectrum 100 CsI DTGS FTIR spectometer with UATR 1 bounce-KRS-5 in the range of 4000–300 cm^{-1}. Elemental analyses (C, H, and N) were performed on a Perkin Elmer 2400 Series II CHNS/O elemental analyzer.

Single-crystal X-ray data of both **1** and **2** were collected at 173(1) K with an Oxford Diffraction Xcalibur diffractometer equipped with a Sapphire3 CCD detector and a graphite monochromator utilizing Mo-Kα radiation (λ = 0.71073 Å). Further details of data collections, structure solutions and refinements are gathered in the ESI. Crystal data and final refinement parameters are shown in Table 1. Selected geometric parameters are gathered

[a] Department of Chemistry, FPV, University of SS Cyril and Methodius, 917 01 Trnava, Slovakia
[b] Department of Inorganic Chemistry, Institute of Chemistry, P. J. Šafárik University in Košice, 041 54 Košice, Slovakia
[c] Instituto de Ciencia de Materiales de Aragón (ICMA), Departamento de Química Inorgánica, University of Zaragoza–CSIC, E-50009 Zaragoza, Spain
[d] Instituto de Síntesis Quimica y Catálisis Homogénea (ISQCH), Departamento de Química Inorgánica, Pedro Cerbuna 12, University of Zaragoza–CSIC, E-50009 Zaragoza, Spain

† Electronic Supplementary Information (ESI) available. CCDC 1523868 and 1523869. For additional crystallographic, spectral and magnetic data see DOI: 10.1039/x0xx00000x.

View Article Online
DOI: 10.1039/C7DT00069C

in Tables 2 and 3 while possible hydrogen bonds are given in Tables S1 and S2 in the ESI. Crystallographic data of compounds **1** and **2** (CCDC 1523868 and 1523869) have been deposited with the Cambridge Crystallographic Data Centre. The molecular graphics were created using Diamond 3.2k software.[15]

Magnetic data were measured on a SQUID magnetometer (MPMS-XL7, Quantum Design) using the RSO mode of detection with *ca* 12 mg for **1** and 26 mg for **2** of the sample encapsulated in a gelatin sample holder. The molar susceptibility χ_{mol} taken at B = 0.01 T and 0.1 T, respectively, was corrected for the underlying diamagnetism. AC susceptibility measurements were done with an oscillating field B_{AC} = 0.38 mT for ten frequencies ranging between ν = 1.1 – 1512 Hz and a temperature interval T = 1.85 – 10.0 K; twenty scans were averaged for each temperature-frequency point. Use of a small DC magnetic field was essential to yield the out-of-phase susceptibility response.

Synthesis

$\{[Dy_2(PDOA)_3(H_2O)_6]\cdot 2H_2O\}_n$ (**1**): To an aqueous solution of $Dy(NO_3)_3$ (0.220 g of the monohydrate, 0.6 mmol, 5 cm^3 of water), an aqueous solution of H_2PDOA (0.203 g, 0.9 mmol, 5 cm^3 of water) mixed with 1.5 cm^3 of aqueous solution of 1 M NaOH (1.5 mmol) were added. The turbidity was filtered from solution; the solution was covered and left for crystallization at room temperature. Colourless crystals of **1** suitable for use in an X-ray study were formed overnight. The crystalline product was separated by filtration followed by washing with distilled water and finally dried in air. Yield: 0.202 g (60 %). Analyses calc. (found) for **1** ($C_{30}H_{40}Dy_2O_{26}$, M = 1141.62 g mol^{-1}): C, 31.56 (31.51); H, 3.53 (3.89) %. FT-IR (in cm^{-1}) for **1**: 3522(w,sh); 3304(m,b); 3087(w); 3070(w); 3005(w); 2964(w); 2935(w); 1676(w); 1604(s); 1580(s); 1499(s); 1433(s); 1413(m); 1342(m); 1334(m); 1294(w); 1259(m); 1245(s); 1230(m); 1195(m); 1158(w); 1133(w); 1122(s); 1070(w); 1047(m); 1030(m); 959(m); 920(m); 824(m); 760(m); 750(s); 722(m); 691(m); 598(s); 584(s); 491(m); 468(m); 378(m); 324(m).

$[Dy_2(PDOA)_3(H_2O)_6]\cdot 3.5H_2O$ (**2**): A mixture of $Dy(NO_3)_3$ (0.073 g of the monohydrate, 0.2 mmol), H_2PDOA (0.068 g, 0.3 mmol), bpy (bpy = 2,2'-bipyridine, 0.031 g, 0.2 mmol), 0.6 cm^3 of 1M aqueous solution of NaOH and 10 cm^3 of water) were placed in a 25 cm^3 glass flask which was closed and heated in the oven at 393 K for 48 hours and then cooled to RT at a rate of 4 deg/h. The resulting turbid solution was filtered and left aside for crystallization, covered with parafilm. Light bluish needles formed within a week and these were separated by filtration and dried in air. Yield: 0.087 g (74 %). Analyses calc. (found) for **2** ($C_{30}H_{43}Dy_2O_{27.5}$, M = 1168.64 g mol^{-1}): C, 30.83 (31.34); H, 3.71 (3.56) %. FT-IR (in cm^{-1}) for **2**: 3519(w,sh); 3274(m,b); 3086(w); 3068(w); 3005(w); 2964(w); 2937(w); 1678(w); 1603(s); 1583(s); 1499(s); 1433(s); 1415(m); 1343(s); 1334(m); 1295(w); 1259(m); 1246(s); 1234(s); 1196(m); 1161(w); 1134(w); 1122(s); 1073(w); 1047(m); 1030(m); 9560(m); 920(w); 824(m); 762(m); 751(s); 722(m); 692(m); 596(s); 584(s); 49(m); 468(m); 377(m); 318(m).

Results and discussion

Syntheses and characterisation

From the reaction system composed of dysprosium nitrate, PDOA and NaOH the previously reported complex **1** with a polymeric crystal structure was isolated under mild conditions and in a higher yield. Modification of the synthetic procedure (use of solvothermal conditions, addition of an auxiliary bpy) led to isolation of the dinuclear complex **2** which, however, did not contain bpy although it could act through its basicity. A similar situation concerning 4,4'-bipyridine was observed during solvothermal syntheses of some lanthanoid complexes.[16] On the other hand, the use of solvothermal conditions and the addition of phen (phen = 1,10-phenantroline) as a blocking ligand led to the isolation of the analogous dinuclear complex $[Dy_2(PDOA)_3(phen)_2(H_2O)_2]\cdot 2H_2O$.[10c]

The IR spectra of both **1** and **2** are rich mainly due to the presence of the PDOA ligand. Due to the complex character of the spectra we limit our discussion to the characteristic absorption bands which were identified using literature data.[17] The most characteristic absorption bands are those originating from asymmetric and symmetric ν(COO) vibrations of the carboxylate groups; these are positioned at 1580 cm^{-1} and 1433 cm^{-1}, respectively, in the spectrum of **1** (1583 and 1433 cm^{-1} in the spectrum of **2**). Weak but easily identifiable are several absorptions at around 3000 cm^{-1}: those above 3000 cm^{-1} (ranges 3087-3005 cm^{-1} for **1** and 3086-3005 cm^{-1} for **2**) can be assigned to $\nu(C_{ar}\text{-}H)$ stretching vibrations, while the bands situated in the spectra of both **1** and **2** slightly below 3000 cm^{-1} may arise from ν(C-H) stretching vibrations of the methylene groups. Broad absorption bands centred around 3301 cm^{-1} with a shoulder at 3522 cm^{-1} (**1**) and centred around 3274 cm^{-1} with a shoulder at 3519 cm^{-1} (**2**), are in accord with the presence of water molecules in the structures of both complexes. Also typical are the strong, sharp absorption bands at 1499 cm^{-1} in the spectra of both complexes **1** and **2**; these corroborate the presence of aromatic rings.

Structure determination

The structure of **1** at 173 K is essentially the same as previously determined at 296 K[9] (Figure 1): the Dy(III) atoms are linked by *syn-anti* carboxylato bridges forming $\{\text{-Dy-O-C-O-}\}_n$ chains and these chains are cross-linked by bis(monodenate) PDOA ligands yielding a ladder-type arrangement (Figure 2). The same type of ladder-like structural arrangement was found in crystal structures of $\{[M_2(PDOA)_3(H_2O)_6]\cdot 2H_2O\}_n$ with other lanthanoids (M = Ce, Sm, Eu, Gd, Tb, Ho, Er.[9,11] It is interesting that within this series of complexes two different packing modes of the ladder-like structural motif were found; as a consequence these complexes crystallize in two different space groups, Pbcn and C2/c, with similar cell dimensions.[9,11]

The unit cell parameters measured at 173 K are somewhat smaller than those measured at room temperature indicating

View Article Online
DOI: 10.1039/C7DT00069C
Dalton Trans ARTICLE

shrinkage of the unit cell volume by 35.9 Å^3. The structure at 173 K has shorter mean Dy-O bonds; the calculated mean values are 2.600 (173 K) *vs* 2.608 (297 K) Å for ether-O atoms, 2.357 *vs* 2.354 Å for carboxylato-O atoms and 2.406 *vs* 2.419 Å for aqua-O atoms.

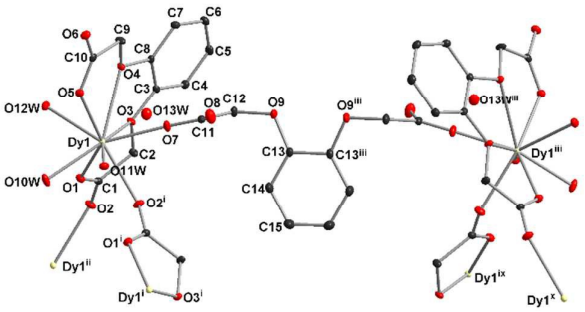

Figure 1. View of the structure of **1** showing the short (Dy1···Dy1^{i}) and long (Dy1 …Dy1^{iii}) bridging of the Dy(III) atoms. The thermal ellipsoids are drawn at 30 % probability level and hydrogen atoms are omitted for clarity. Symmetry codes: (i) x, 1-y, z-1/2; (ii) x, 1-y, z+1/2; (iii) 1-x, y, 1/2-z.

Table 1. Crystal data and results of refinement for **1** and **2**

Compound		**1**	**2**
Empirical formula		C15 H20 Dy O13	C30 H43 Dy2 O27.5
Formula weight M_r		570.81	1168.64
Temperature [K]		173(1)	173(1)
Wavelength [Å]		Mo$K\alpha$, 0.71073	Mo$K\alpha$, 0.71073
Crystal system		Orthorhombic	Orthorhombic
Space group		*Pbcn*	*Pbca*
Unit cell parameters	*a* [Å]	34.0219(7)	16.3718(5)
	b [Å]	12.6029(3)	7.9713(3)
	c [Å]	8.2935(2)	30.9027(12)
Volume [Å^3]		3556.01(13)	4032.9(3)
Z		8	4
Density (calc.) [Mg/m^3]		2.132	1.925
Abs. coef., μ [mm^{-1}]		4.28	3.775
Crystal colour / shape		colourless plate	bluish needle
Crystal size [mm^3]		0.29×0.18×0.03	0.013x0.039x0.267
θ range for data collection [°]		4.20-27.50	3.46 – 27.50
Index range for data collection [°]		h = -43 → 44	h = -21→ 11
		k = -16 → 16	k = -8 → 10
		l = -10 → 10	l = -40 → 40
Reflections collected		42 072	19 610
Independent reflexions (R_{int})		4078 (0.0327)	4632 (0.0603)
Observed reflexions [I>2σ_I]		3768	3520
Data / restraints / parameters		4078 / 0 / 294	4632 / 7 / 349
Goodness-of-fit on F^2		1.045	1.129
Final R indices [I>2σ_I]	$R1$	0.0194	0.0387
	$wR2$	0.0427	0.0762
Final R indices (all)	$R1$	0.0218	0.0584
	$wR2$	0.0438	0.0822
Diff. peak and hole [e.Å^{-3}]		0.895; -0.575	0.873; -1.284

The central Dy(III) atom in **1** is nona-coordinated by four oxygen atoms from pentadentate PDOA ligand, two oxygen atoms from bridging functions of neighbouring PDOA ligands and three aqua ligands (donor set $O_4O_2O_3$) (Figure 3, left) and its coordination polyhedron can be described as close to a spherical capped square antiprism as indicated by the programme SHAPE.[18]

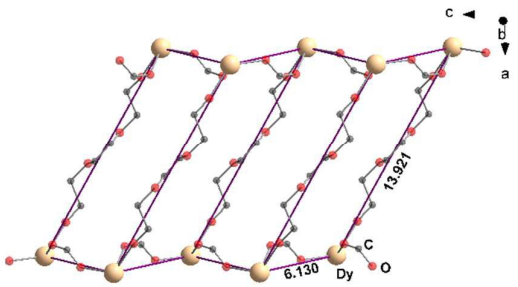

Figure 2. Ladder-like arrangement of the Dy(III) atoms in **1**. Among the carbon and oxygen atoms are shown only those participating in bridging the Dy(III) atoms.

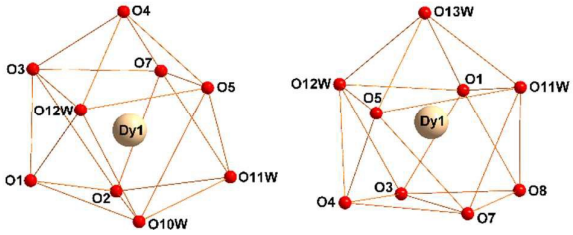

Figure 3. Coordination polyhedra of the Dy(III) central atoms in **1** (left) and in **2** (right).

The molecular structure of **2** consists of dinuclear $[Dy_2(PDOA)_3(H_2O)_6]$ units with a local arrangement similar to that of **1** (Figure 4). Contrary to **1**, one PDOA ligand behaves only as a tetradentate chelating blocking ligand with no additional bridging function, thus limiting the dimensionality of the structure; the second PDOA ligand, similarly to that in **1**, interlinks two Dy(III) atoms but in a bis(chelate) fashion. Similar bridging was found in the analogous dinuclear complex $[Dy_2(PDOA)_3(phen)_2(H_2O)_2]\cdot 2H_2O$.[10c] We note that the bridging PDOA in **2** is disordered over two positions (about a centre of symmetry) with equal occupancies for the two positions (see Figure S3 in the ESI). The mean values of Dy-O bonds are (the values in the parentheses are that of **1**) 2.546 Å (2.600) for ether-O atoms, 2.390 Å (2.357) for carboxylato-O atoms and 2.369 Å (2.372) for aqua-O atoms. These results show that in **2** the mean Dy-O bond with ether O-atoms is somewhat shorter, while the mean Dy-O bond with carboxylate–O atoms is somewhat longer; almost the same mean Dy-O bonds with aqua ligands were found in both complexes **1** and **2**. The observed differences may be ascribed to differences in the coordination modes of the PDOA ligand in both complexes.

Each of the Dy(III) atoms in **2** is nona-coordinated by four oxygen atoms from a tetradentate chelating PDOA ligand, two oxygen atoms from the chelating carboxylate group of the bridging PDOA ligand and three aqua ligands, yielding a donor set $O_4O_2O_3$. The coordination polyhedron, similar to that of **1**, is close to a spherical capped square antiprism (Figure 3, right) as suggested by the

View Article Online
DOI: 10.1039/C7DT00069C

program SHAPE.[18] This finding corroborates the close similarity of **1** and **2** at the level of their core structures despite the difference in the coordination of the bridging PDOA ligand.

A common feature of both complexes **1** and **2** is the presence of aqua ligands and water solvate molecules, which are involved in an extended network of hydrogen bonds of the OH···O type; the carboxylate oxygen atoms are also involved in these (Figures S1 and S4, Tables S1 and S2 in the ESI). The intermolecular hydrogen bonds in both **1** and **2** are important also from the point of view of their magnetic properties, as they ensure relative proximity of the neighbouring Dy(III) atoms (Figures S2 and S5 in the ESI); this feature in connection with the observed magnetic properties is discussed below.

Table 2. Selected geometric parameters [Å,°] for **1**.

Dy1—O1	2.3958(17)	Dy1—O7	2.2652(17)
Dy1—O2^{i}	2.3856(17)	Dy1—O10W	2.3195(19)
Dy1—O3	2.5530(17)	Dy1—O11W	2.4143(18)
Dy1—O4	2.6477(16)	Dy1—O12W	2.4852(18)
Dy1—O5	2.3799(16)		
O1—Dy1—O2^{i}	71.58(6)	O2^{i}—Dy1—O3	89.74(6)
O1—Dy1—O3	61.97(5)	O3—Dy1—O4	59.18(5)
O1—Dy1—O4	113.17(5)	O4—Dy1—O5	62.49(5)
O1—Dy1—O5	140.51(6)	O5—Dy1—O7	90.87(6)
O1—Dy1—O7	124.64(6)	O7—Dy1—O10W	148.91(7)
O1—Dy1—O10W	70.11(6)	O10W—Dy1-O11W	68.66(7)
O1—Dy1—O11W	127.69(6)	O10W—Dy1—O12W	74.73(7)
O1—Dy1—O12W	69.95(6)	O11W—Dy1—O12W	125.71(6)

Symmetry code: (i) x, 1-y, z-1/2.

Table 3 Selected geometric parameters [Å, º] for **2**.

Dy1-O1	2.345(3)	Dy1-O8	2.497(3)
Dy1-O3	2.516(3)	Dy1-O11W	2.370(4)
Dy1-O4	2.575(3)	Dy1-O12W	2.364(4)
Dy1-O5	2.316(3)	Dy1-O13W	2.372(4)
Dy1-O7	2.401(4)		
O1-Dy1-O3	65.10(11)	O3-Dy1-O4	60.34(10)
O1-Dy1-O4	122.75(12)	O4-Dy1-O5	63.89(12)
O1-Dy1-O5	153.87(13)	O5-Dy1-O7	80.65 (13)
O1-Dy1-O7	125.47(12)	O7-Dy1-O11W	75.90(14)
O1-Dy1-O8	72.67(12)	O11W-Dy1-O12W	141.00(15)
O1-Dy1-O11W	96.32(13)	O11W-Dy1-O13W	70.51(15)
O1-Dy1-O12W	75.37(14)	O12W-Dy1-O13W	70.57(15)
O1-Dy1-O13W	81.29(14)		

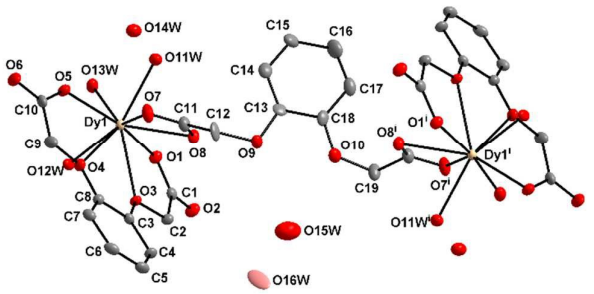

Figure 4. View of the molecular structure of **2** along with atom numbering scheme. The thermal ellipsoids are drawn at 30 % probability level. Hydrogen atoms are omitted for clarity. Only one of the two symmetry related disordered position of the bridging PDOA ligand associated with the disorder of solvate water molecules O15W (sof = 0.5) and O16W (sof=0.25) is shown (the positional disorder is fully depicted in Figure S3). Symmetry code: i: -x, 1-y, 1-z.

Magnetic Data

DC magnetic data

The DC magnetic functions of **1** are displayed in Figure 5. The room-temperature value of the dimensionless product function amounts to $\chi T/C_0$ = 71.3 whereas the high-temperature limit is $(\chi T/C_0)_{HT} = 2g_J^2 J_{max}(J_{max} + 1)/3 = 75.5$ for g_J = 4/3 of the $^6H_{15/2}$ ground multiplet (the reduced Curie constant $C_0 = N_A\mu_0\mu_B^2/k_B = 4.7142\times10^{-6}$ m^3 K mol^{-1} involves physical constants with their usual meanings). A slight antiferromagnetic interaction is indicated as the product function decreases on cooling; at low temperature a depopulation of the multiplets split by the crystal-field (Stark levels) is evidenced.

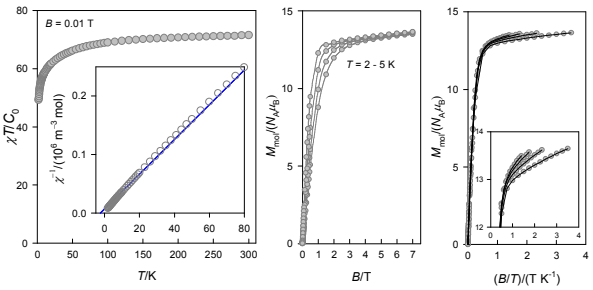

Figure 5. Magnetic functions for **1**. Left – temperature dependence of the dimensionless product function $\chi T/C_0$ (inset – temperature dependence of the inverse molar magnetic susceptibility), centre – field dependence of the magnetization, right – *M vs B/T* plot (inset – zoomed).

The magnetization per formula unit $M_1 = M_{mol}/N_A\mu_B$ rises rapidly with the applied field and confirms high magnetic anisotropy. However, the saturation value at T = 2.0 K and B = 7 T is only M_1 = 13.6 as opposed to the theoretical limit of $M_1 = 2g_{Dy}J_{max} = 20$. The DC magnetic data for **2** indicates high magnetic anisotropy as well (Figure 6) combined with an exchange interaction of an antiferromagnetic nature (see ESI).

View Article Online
DOI: 10.1039/C7DT00069C
Dalton Trans ARTICLE

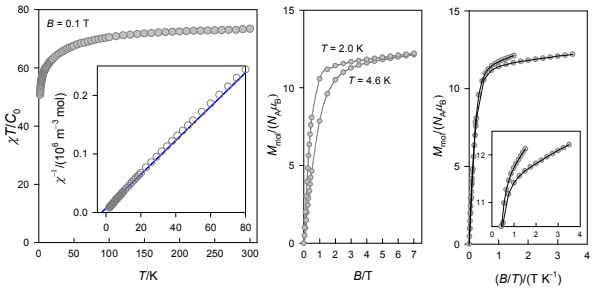

Figure 6. Magnetic functions for **2**.

AC magnetic data for 1

The AC susceptibility measurements for **1** at T = 2.0 K show that the out-of-phase component is absent at zero field (Figure 7). However, with an applied DC field it grows, passes through a maximum between 0.05 and 0.2 T (depending upon the frequency of the oscillating AC field) and then decays continuously. This data confirms that **1** exhibits a field-supported slow magnetic relaxation.

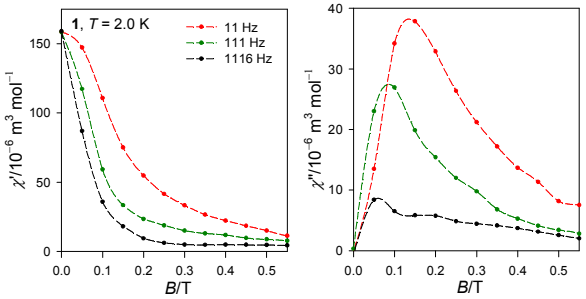

Figure 7. The in-phase χ' and out-of-phase χ'' molar susceptibility (SI units) for **1** as a function of the external DC magnetic field at T = 2.0 K. Lines serve as a visual guide.

Temperature dependence of the AC susceptibility components shows that the superparamagnetism survives until T = 9 K (see ESI).

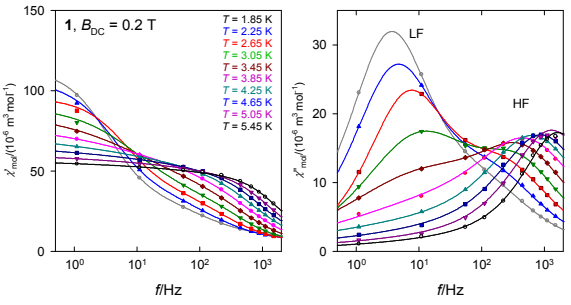

Figure 8. Frequency dependence of the AC susceptibility for **1** at B_{DC} = 0.2 T. Left – the in-phase component; right – the out-of-phase component. Solid lines – fitted with the two-set Debye model.

A plot of the magnetic data as a function of the frequency at constant temperature is given in Figure 8. The out-of phase susceptibility evidences the presence of two relaxation channels: one dominates at low frequency (LF) and diminishes progressively with temperature, whereas the second one applies at higher frequencies (HF); they coexist equally at *ca* 3 K. An extended two-set Debye model was used in interpreting the frequency dependence of the AC magnetic susceptibility[1]

$$\tilde{\chi}(\omega) = \chi_S + (\chi_{T1} - \chi_S)/[1 + (i\omega\tau_1)^{1-\alpha_1}] + (\chi_{T2} - \chi_{T1})/[1 + (i\omega\tau_2)^{1-\alpha_2}]$$

where two relaxation times (τ_1, τ_2) and two distribution parameters (α_1, α_2) occur along with two isothermal susceptibilities (χ_{T1}, χ_{T2}) and the adiabatic susceptibility (χ_S); ω = 2πf. This equation decomposes into two components χ' and χ'' as shown in the ESI. The fitting procedure was based upon minimization of a joint functional $F = R(\chi') \times R(\chi'')$ that accounts uniformly to relative errors of both data sets. Twenty frequency points (ten for χ' and ten for χ'') ensure a reliable determination of seven varied parameters. The quality of the fit is assessed by the discrepancy factors R and the standard deviations for each varied parameter. The results in numerical form are listed in the ESI, and it can be seen that the resulting parameters vary systematically with temperature. The final parameters were used in generating extrapolation and interpolation lines that are plotted in Figure 8.

By plotting χ'' *vs* χ' for a set of fixed temperatures, the Argand (Cole-Cole) diagram has been constructed – Figure 9. This, in fact, refers to two overlapping arcs possessing either one dominant part with a shoulder and/or two visible maxima.

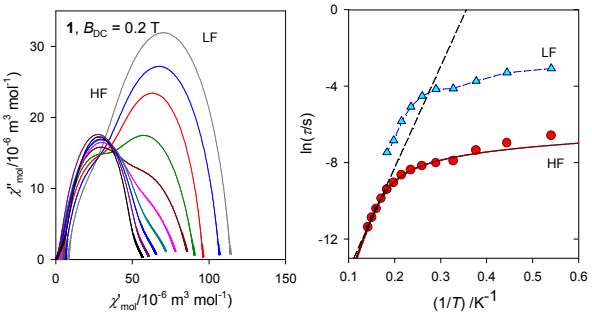

Figure 9. The AC susceptibility data for **1** at B_{DC} = 0.2 T. Left – Argand plot (fixed temperature, colour code according to Figure 8); right – Arrhenius-like plot. Solid lines – fitted. Dashed straight line – fit to the Arrhenius equation.

The temperature evolution of the relaxation time for the high-spin branch has been fitted by an extended relaxation equation

$$\tau^{-1} = \tau_0^{-1} \exp(-U/k_B T) + AB^m T + CT^n + D_t$$

where the barrier to spin reversal U and the extrapolated relaxation time τ_0 refer to the Orbach process; A characterizes the direct process, C – the Raman process, and eventually D_t – the temperature-independent quantum tunnelling. The resulting set of parameters is listed in Table 4. It can be compared with the linear fit of three high-temperature data points to a simple Arrhenius equation (this set is less reliable).

View Article Online
DOI: 10.1039/C7DT00069C

Table 4. Fitted relaxation parameters

Parameter	**1**, B_{DC} = 0.2 T	**2**, B_{DC} = 0.2 T
a) Non-linear fit of all data		
U/k_B /K	71.6(33)	97.8(25)
τ_0 /10^{-10} s	6.3(26)	0.24(8)
A /10^4 T^{-2} K^{-1} s^{-1}, m = 2	1.63(21)	1.66(8)
C /K^{-5} s^{-1}, n = 5	1.21(24)	1.88(7)
R /%	1.4	0.66
b) Linear fit of HT data		
U/k_B /K	53.1	55.6
τ_0 /10^{-10} s	62.7	48.9

In summary, the AC susceptibility data for **1** confirm the presence of two relaxation channels that coexist at low temperature. The LF relaxation time at B_{DC} = 0.2 T and T = 1.85 K is as slow as τ(LF) = 46(1) ms whereas the HF one is τ(LF) = 1.4(2) ms. The barrier to spin reversal obtained from the non-linear fit of the Arrhenius-like plot is U/k_B = 72 K. At low temperature the Raman and the direct process of the relaxation take on significance. Isothermal and adiabatic susceptibilities can be used in calculating the low (high)-frequency mole fraction at the given temperature: $x_{LF} = (\chi_{LF} - \chi_S)/(\chi_{HF} - \chi_S)$. This is x_{LF} = 0.76 at T = 1.85 K and it gradually decreases to x_{LF} = 0.29 at T = 5.45 K (above this temperature the LF peak is not resolved satisfactorily).

The existence of manifold relaxation channels has already been reported for a number of examples including not only Dy(III) complexes (Table 5),[7c,14c,19] but also Co(II), Ni(II) and Cu(II) compounds.[14a,14b,20] There is speculation that the existence of multiple relaxation processes is associated with the presence of inequivalent crystallographic centres. Even if the two centres have the same local environment, the faster, high-frequency relaxation could be associated with individual centres whereas the slower, low-frequency regime can be associated with a kind of coupling (exchange, phonon, through π-π stacking, π-H interaction, etc.). The application of a small DC field (B_{DC} = 0.1 – 0.2 T) is essential in suppressing the magnetic tunnelling mechanism which gives a much faster relaxation. Some more data can be extracted from recent reviews.[21]

Table 5. Selected examples of Dy-containing single-molecule magnets with multiple relaxation channels

Complex of Dy^{III}	B_{DC} / T	Channel	(U/k_B) / K	τ_0 / s	Ref.
$[Dy_2]^1_\infty$	0.2	HF [a]	71.6	6.3×10^{-10}	This work
$[Dy_2]$	0.2	HF [a]	97.8	2.4×10^{-11}	This work
d-$[Dy]_2$	0.1	HF	46.1	6.4×10^{-6}	19a
		LF	36.5	7.9×10^{-7}	
l-$[Dy]_2$	0.1	HF	49.3	4.8×10^{-6}	19a
		LF	37.0	7.7×10^{-7}	
$[Co^{II}_2Dy_2]$	0	HF	82.1	6.2×10^{-7}	19b
		LF	11.0	7.7×10^{-4}	
$[Dy_4]$	0	HF	54.2	7.2×10^{-7}	19c
		LF	16.8	1.4×10^{-6}	
$[Co^{II}_2Dy_{10}]$	0	HF	25	3.1×10^{-6}	19d
		LF	4.3	1.1×10^{-4}	
$[Ni^{II}_2Dy_2]^1_\infty$	0.1	HF	17.4	7.7×10^{-7}	7c
$[Zn^{II}_2Dy_2]$	0	HF	47.9	2.7×10^{-7}	19e
$[Cu^{II}Dy]$	0.2	HF [a]	122	9.9×10^{-7}	19f
$[Co^{III}Dy]$	0.2	HF [a]	113	7.0×10^{-9}	19f
$[Co^{III}Dy]$	0.1	HF [a]	17.6	2.5×10^{-6}	14c
	0.2	HF [a]	25.6	4.7×10^{-7}	14c
	0.3	HF [a]	29.5	1.1×10^{-7}	14c

[a] Resulting from the non-linear fit to the curved Arrhenius-like plot.

There is a curvature in the Arrhenius plot for the HF process when approaching the lowest temperatures of the experiment. This is associated with the Raman and direct processes along with the onset of the tunnelling mechanism. An analogous interpretation has been presented for the $[Ni^{II}_2Dy_2]^1_\infty$ system formed by a ladder-like complex $[Ni_2(H_2O)_2(valpn)_2Dy_2(tfa)_3]_n \cdot 4nCH_3CN$ ($valpn^{2-}$ = the dianion of the Schiff base formed by the reaction of *o*-vanillin with 1,3-propanediamine; $pdca^{2-}$ = 2,6-pyridinedicarboxylato; tfa^{2-} = terephthalato) where, however, only a single relaxation channel has been reported.[7c] On the contrary, for the ($[Co^{II}_2Dy_2]$ system formed by the complex $[Co_2Dy_2(L)_4(NO_3)_2(THF)_2] \cdot 4THF$ (H_2L is a Schiff base formed by the reaction of *o*-vanillin with 2-aminophenol) two distinct relaxation channels were identified.[19b]

The behaviour of **1** in this study accredits its classification as a single molecule magnet. On the other hand, the single chain magnets possess much faster relaxation time and the Glauber type of dynamics.[22]

The AC susceptibility data for **2** (Figures 10 and 11) are analogous to those for **1**; however, some differences are evident. First, the out-of phase susceptibility signal disappears at ca 9 K for both analogous complexes (see the ESI). The profiles of the χ'' *vs* B_{DC} curves [T = 2.0 K], however, are different. The positions of the LF peaks at χ'' is moved to lower frequencies, implying a prolongation of the relaxation time for this channel. The SMM parameters for **2** are τ(LF) = 183(8) ms and τ(HF) = 1.0(1) ms at T = 1.9 K; U/k_B = 98 K. The low-frequency mole fraction at T = 1.9 K is x_{LF} = 0.69 and this gradually decreases to x_{LF} = 0.04 at T = 7.1 K.

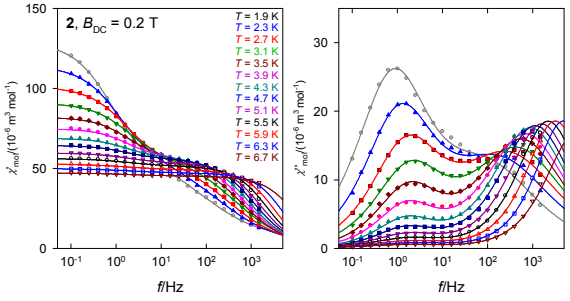

Figure 10. Frequency dependence of the AC susceptibility for **2** at B_{DC} = 0.2 T. Left – the in-phase component; right – the out-of-phase component. Solid lines – fitted with the two-set Debye model.

View Article Online
DOI: 10.1039/C7DT00069C
Dalton Trans ARTICLE

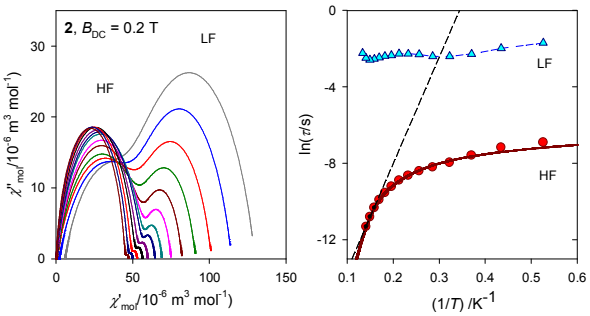

Figure 11. The AC susceptibility data for **2** at B_{DC} = 0.2 T. Left – Argand plot (fixed temperature); right – Arrhenius-like plot. Solid lines – fitted. Dashed straight line – fit to the Arrhenius equation.

It is interesting to note that despite the different structural dimensionalities of **1** and **2** based on covalent bonds only (ladder-like arrangement *vs* dinuclear molecules) they display some similarities at the packing level as in both structures sheets formed by relatively closely positioned Dy(III) atoms can be distinguished (see Figure S6 and Figure S7 in the ESI). In **1,** within these sheets parallel to the *bc* plane the Dy(III) separations are 6.1304(3) (carboxylato bridge) and 6.6340(7) Å (hydrogen bonded atoms). On the other hand, in **2** a similar sheet-like arrangement can be observed in which the nearest Dy(III) atoms at distances of 6.4074(7) and 7.5953(5) Å interact only via hydrogen bonds. This structural similarity (and quantitative differences within this similarity) may lead to the observed similarity and quantitative differences in magnetic behaviour of the two analogues **1** and **2**.

In summary, the Dy(III) ions seem to be weakly coupled but there is some canting between their easy axes due to the zigzag orientations. When the magnetic field is applied, the spins are decoupled and then aligned (in the antiferromagnetic case). Basically any slow relaxation in zero field is not seen because the system displays strong quantum tunnelling of magnetization or/and coupling. In an applied field the probability of the tunnelling is decreased. At the same time two relaxation modes are seen, which probably arise from a mononuclear Dy SMM and also at lower temperature from two or more $\{Dy\}_n$ SMMs that are weakly coupled into finite blocks. With increasing temperature the weakly coupled oligomers disintegrate to monomers and thus the LF relaxation channel vanishes.

Conclusions

The structure of two isomers of $[Dy_2(PDOA)_3(H_2O)_6]\cdot 2H_2O$ (H_2PDOA = 1,2-phenylenedioxydiacetic acid) has been determined by X-ray structure analysis. Whereas the polymeric form **1** refers to an infinite ladder-type complex, the dinuclear species **2** is a molecular complex. DC magnetic data confirm a sizable magnetic anisotropy. Both species exhibit a slow magnetic relaxation supported by a small external magnetic field. There are two relaxation channels: low-frequency and high frequency ones with the relaxation time of the order of a few ms at low temperature. In order to obtain a better insight into the relationship between the structural parameters and the phenomenon of slow magnetic relaxation we intend to study further Dy(III) complexes based on PDOA ligand with the aim to tune its magnetic properties through small structural changes.

Acknowledgements

Grant agencies (Slovakia: VEGA 1/0534/16, 1/0063/17 and 1/0131/16, and APVV-14-0078; Spain: MAT2015-68200-C2-1-P by the Ministerio de Ciencia e Innovación, European Union Regional Development Fund, FEDER, and Diputación General de Aragón (M4) are acknowledged for their financial support. The authors thank Prof. R. Clérac (University of Bordeaux) for valuable comments on an early version of the manuscript.

References

1 D. Gatteschi, R. Sessoli, J. Villain, *Molecular Nanomagnets*, Oxford University Press, Oxford, 2006.
2 D.N. Woodruff, R. E. P. Winpenny and R. A. Layfield, *Chem. Rev.* 2013, **113**, 5110.
3 Y.-S. Meng, S.-D. Jiang, B.-W. Wang and S. Gao, *Acc. Chem. Res*., 2016, **49**, 2381.
4 (a) S.-D. Jiang, B.-W. Wang, G. Su, Z.-M. Wang and S. A. Gao, *Angew. Chem., Int. Ed.* 2010, **49**, 7448; (b) W.-B. Sun, B. Yan, Y.-Q. Zhang, B.-W. Wang, Z.-M. Wang, J.-H. Jia and S. Gao, *Inorg. Chem. Front*., 2014, **1**, 503; (c) E. Mamontova, J. Long, R. A. S. Ferreira, A. M. P. Botas, D. Luneau, Y. Guari, L. D. Carlos and J. Larionova, *Magnetochem*., 2016, **2**, Art. N. 41.
5 (a) K. Zhang, D. Liu, V. Vieru, B. Cui, F.-S. Guo, L. F. Chibotaru and Y.-Y. Wang, *Dalton Trans*., 2017, **46**, 638; (b) J. Long, F. Habib, P.-H. Lin, I. Korobkov, G. Enright, L. Ungur, W. Wernsdorfer, L. F. Chibotaru and M. Murugesu, *J. Am. Chem. Soc*., 2011, **133**, 5319; (c) J. Zhang, H.-F. Zhang, Y.-M. Chen, X.-F. Zhang, Y.-H. Li, W. Liu and Y.-P. Dong, *Dalton Trans*., 2016, **45**, 16463.
6 (a) M. U. Anwar, L. K. Thompson, L. N. Dawe, F. Habib and M. Murugesu, *Chem. Commun*., 2012, **48**, 4576; (b) P.-H. Lin, I. Korobkov, W. Wernsdorfer, L. Ungur, L. F. Chibotaru and M. Murugesu, *Eur. J. Inorg. Chem*., 2011, 1535; (c) Q. Chen, J. Li, Y.-S. Meng, H.-L. Sun, Y.-Q. Zhang, J.-L. Sun and S. Gao, *Inorg. Chem.*, 2016, **55**, 7980; (d) T. Lacelle, G. Brunet, A. Pialat, R. J. Holmberg, Y. Lan, B. Gabidullin, I. Korobkov, W. Wernsdorfer and M. Murugesu, *Dalton Trans*., in press (DOI: 10.1039/C6DT04413A).
7 (a) G. Poneti, K. Bernot, L. Bogani, A. Caneschi, R. Sessoli, W. Wernsdorfer and D. Gatteschi, *Chem. Commun*., 2007, 1807; (b) V. Chandrasekhar, B. M. Pandian, J. J. Vittal and R. Clérac, *Inorg. Chem*., 2009, **48**, 1148; (c) T. D. Pasatoiu, M. Etienne, A. M. Madalan, M. Andruh and R. Sessoli, *Dalton Trans*., 2010, **39**, 4802; (d) S.-Y. Jhan, S.-H. Huang, C.-I. Yang and H.-L. Tsai, *Polyhedron*, 2013, **66**, 222.
8 J. Liu, Y.-C. Chen, J.-L.; Liu, V. Vieru, L. Ungur, J.-H. Jia, L. F. Chibotaru, Y. Lan, W. Wernsdorfer, S. Gao, X.-M. Chen and M.-L. Tong, *J. Am. Chem. Soc*., 2016, **138**, 5441.
9 X. Li, X.-S. Wu, H.-L. Sun, L.-J. Xu and G.-Fu Zi, *Inorg. Chim. Acta*, 2009, **362**, 2837.
10 (a) Y. Jiang, X.-S. Wu, X. Li, J.-H. Song and Y.-Q. Zou, *J. Coord. Chem*., 2010, **63**, 36; (b) H. B. Kerfoot, G. R. Choppin and T. J. Kistenmacher, *Inorg. Chem.*, 1979, **18**, 787; (c) X. Li, Y.-Q. Li, X.-J. Zheng and H.-L. Sun, *Inorg. Chem. Commun*., 2008, **11**, 779;

View Article Online
DOI: 10.1039/C7DT00069C

11 (a) P. Gawryszewska and Z. Ciunik, *J. Photochem. Photobiol. A: Chemistry*, 2009, **202**, 1; (b) M. Stolárová, J. Černák, M. Tomás, I. Ara, L. R. Falvello, R. Boča and J. Titiš, *J. Coord. Chem*., 2014, **67**, 1046; (c) T. Behrsing, G. B. Deacon, P. C. Junk, B. W. Skelton, A. N. Sobolev and A. H. White, *Z. Anorg. Allg. Chem*., 2013, **639**, 41.
12 M. Stolárová, J. Černák, M. Tomás, I. Ara, M. Orendáč and L. R. Falvello, *Polyhedron*, 2015, **88**, 149.
13 X.-F. Li and Z.-B. Han, *Acta Crystallogr*., 2006, **E62**, m2024.
14 (a) R. Boča, J. Miklovič and J. Titiš, *Inorg. Chem*., 2014, **53**, 2367; (b) J. Miklovič, D. Valigura, R. Boča and J. Titiš, *Dalton Trans*., 2015, **44**, 12484; (c) S. Hazra, J. Titiš, D. Valigura, R. Boča and S. Mohanta, *Dalton Trans*., 2016, **45**, 7510; (d) L. Smolko, J. Černák, M. Dušek, J. Titiš and R. Boča, *New J. Chem*., 2016, **40**, 6593.
15 Diamond - Crystal and Molecular Structure Visualization Crystal Impact - Dr. H. Putz & Dr. K. Brandenburg GbR, Kreuzherrenstr. 102, 53227 Bonn, Germany.
16 J.-C. Jin, W.-Q. Tong, A.-Y. Fu, C.-G-. Xie, W.-G. Chang, J. Wu, G.-N. Xu, Y.-N. Zhang, Y. Li and P.-Q. Yang, *J. Sol. State Chem*., 2015, **225**, 2016.
17 K. Nakamoto, Infrared and Raman Spectra of Inorganic and Coordination Compounds, Part B: Applications in Coordination, Organometallic, and Bioinorganic Chemistry, 6th Ed., Wiley, New York, 1997.
18 M. Llunell, D. Casanova, J. Cirera, P. Alemany and S. Alvarez, SHAPE – Program for the Stereochemical Analysis of Molecular Fragments by Means of Continuous Shape Measures and Associated Tools, Version 2.1, University of Barcelona, Spain, 2013.
19 (a) C.-M. Liu, D.-Q. Zhang and D.-B. Zhu, *Inorg. Chem*., 2013, **52**, 8933. (b) K. C. Mondal, A. Sundt, Y. Lan, G. E. Kostakis, O. Waldmann, L. Ungur, L. F. Chibotaru, C. E Anson and A. K. Powell, *Angew. Chem. Int. Ed*., 2012, **51**, 7550. (c) V. Chandrasekhar, S. Hossain, S. Das, S. Biswas and J.-P. Sutter, *Inorg. Chem*., 2013, **52**, 6346. (d) L.-F. Zou, l. Zhao, Y.-N. Guo, G.-M. Yu, Y. Guo, J. Tang and Y.-H. Li, *Chem. Commun*., 2011, **47**, 8659; (e) S. M. T. Abtab, M. C. Majee, M. Maity, J. Titiš, R. Boča and M. Chaudhury, *Inorg. Chem*., 2014, **53**, 1295; (f) M. Dolai, M. Ali, J. Titiš and R. Boča, *Dalton Trans*., 2015, **44**, 13242.
20 (*a*) L. Smolko, J. Černák, J. Dušek, J. Miklovič, J. Titiš and R. Boča, *Dalton Trans.*, 2015, **44**, 17565; (*b*) C. Rajnák, J. Titiš, O. Fuhr, M. Ruben and R. Boča, *Inorg. Chem.*, 2014, **53**, 8200; (*c*) C. Rajnák, A. Packová, J. Titiš, J. Miklovič, J. Moncoľ and R. Boča, *Polyhedron*, 2016, **110**, 85. (*d*) A. Packová, J. Miklovič and R. Boča, *Polyhedron*, 2015, **102**, 88; (*e*) W. Huang, T. Liu, D. Wu, J. Cheng, Z. W. Ouyang and C. Duan, *Dalton Trans.*, 2013, **42**, 15326; (*f*) R. Boča, C. Rajnák, J. Titiš and D. Valigura, *Inorg. Chem*., 2017, **56**, in press
21 (*a*) G. A. Craig and M. Murrie, *Chem. Soc. Rev*., 2015, **44**, 2135, and references therein; (b) S. Gómez-Coca, D. Aravena, R. Morales and E. Ruiz, *Coord. Chem. Rev*., 2015, **289-290**, 379, and references therein; (c) J. M. Frost, K. L. M. Harriman and M. Murugesu, *Chem. Sci*., 2016, **7**, 2470, and references therein.
22 C. Coulon, H. Miyasaka and R. Clérac, *Struct. Bonding*, 2006, **122**, 163.